Spatial intensity correlation and aperture averaging measurements in a 20 mile retro-reflected lasercom link

Christopher I. Moore[a], Harris R. Burris[b], Michele R. Suite[a], Mena F. Stell[b], Michael J. Vilcheck[a], Mark A. Davis[c], Rita Mahon[d], William S. Rabinovich[e], G. Charmaine Gilbreath[f], Eun Oh[f], William J. Scharpf[a], and Anne E. Reed[a]

[a]U.S. Naval Research Laboratory, Code 8123, Advanced Systems Technology Branch, 4555 Overlook Ave SW, Washington, DC 20375

[b]Research Support Instruments, Inc., 4325-B Forbes Boulevard, Lanham, MD 20706

[c]Honeywell T.S.I., 7515 Mission Drive, Lanham, MD 20706

[d]Jaycor/Titan Inc., 1410 Spring Hill Road, McLean, VA 22102

[e]U.S. Naval Research Laboratory, Code 5654, Photonics Technology Branch, 4555 Overlook Ave SW, Washington, DC 20375

[f]U.S. Naval Research Laboratory, Code 7215, Radio/IR/Optical Sensors Branch, 4555 Overlook Ave SW, Washington, DC 20375

ABSTRACT

The Naval Research Laboratory has established a lasercom test bed across the Chesapeake Bay. The test bed uses a bi-static transmitter/receiver arrangement on the western shore of the Chesapeake Bay and various configurations of 5 cm retro-reflectors on the eastern shore to produce a 32 km retro-reflected lasercom test range. Experiments measuring the laser's transverse spatial profile after propagation over the test range have been performed. These experiments use an InGaAs CCD to image the pupil plane of the 40 cm receiver telescope and a frame grabber to store contiguous images for analysis. Analysis of these image sequences allows measurement of transverse spatial correlations across the received beam after 32 km retro-reflected propagation of the beam. Various configurations and numbers of retro-reflectors were studied to investigate the impact of number and arrangement of retro-reflectors on the received beam's spatial profile and spatial correlations. Additionally, since the CCD output is stored as a contiguous stream of images, analysis of these images' intensity variance in time allows measurement of aperture averaging effects as a function of number of retro-reflectors and their geometry. Results from these experiments are presented.

Keywords: Free space lasercom, spatial coherence, spatial correlations, aperture averaging, free-space optical communications, scintillation

1. INTRODUCTION

The Naval Center for Space Technology (NCST) at the United States Naval Research Laboratory (NRL) has established a long range free space laser communication (lasercom) test range over the Chesapeake Bay for maritime testing of lasercom components. The test bed consists of a bi-static transmitter/receiver on the western shore of the Chesapeake Bay at NRL's Chesapeake Bay Detachment (NRL-CBD) and various configurations of retro-reflectors on Tilghman Island on the eastern shore of the Chesapeake Bay. The range is almost exclusively over water with only a few meters of land on either end and 16.2 km of water in the middle resulting in a 32.4 km round trip propagation path. Typical values of the atmospheric structure constant, C_n^2, over the test range are between 10^{-15} and 10^{-14}, corresponding to Rytov variances from 10 to 100.[1] The test range is therefore a strong turbulence environment, which is ideal for testing lasercom components and techniques suitable for ship-to-ship communications. Additionally, laser beam degradation after propagation over the test range is typically worse than beam degradation induced over ground-to-space links making the test range a worst case test bed for ground to satellite lasercom testing.

A number of experiments have been performed over the test range including bit-error-rate testing at 622 Mbps,[2] long term angle-of-arrival fluctuation based turbulence monitoring,[1] and fast steering mirror correction for angle of

Free-Space Laser Communication and Active Laser Illumination III, edited by David G. Voelz, Jennifer C. Ricklin, Proc. of SPIE Vol. 5160 (SPIE, Bellingham, WA, 2004) · 0277-786X/04/$15 · doi: 10.1117/12.507864

Report Documentation Page

Form Approved
OMB No. 0704-0188

1. REPORT DATE	2. REPORT TYPE	3. DATES COVERED
2004		**00-00-2004 to 00-00-2004**

4. TITLE AND SUBTITLE	5a. CONTRACT NUMBER
Spatial intensity correlation and aperture averaging measurements in a 20 mile retro-reflected lasercom link	5b. GRANT NUMBER
	5c. PROGRAM ELEMENT NUMBER
6. AUTHOR(S)	5d. PROJECT NUMBER
	5e. TASK NUMBER
	5f. WORK UNIT NUMBER
7. PERFORMING ORGANIZATION NAME(S) AND ADDRESS(ES) **Naval Research Laboratory,Code 8123,4555 Overlook Avenue, SW,Washington,DC,20375**	8. PERFORMING ORGANIZATION REPORT NUMBER
9. SPONSORING/MONITORING AGENCY NAME(S) AND ADDRESS(ES)	10. SPONSOR/MONITOR'S ACRONYM(S)
	11. SPONSOR/MONITOR'S REPORT NUMBER(S)

12. DISTRIBUTION/AVAILABILITY STATEMENT
Approved for public release; distribution unlimited

13. SUPPLEMENTARY NOTES

14. ABSTRACT

15. SUBJECT TERMS

16. SECURITY CLASSIFICATION OF:			17. LIMITATION OF ABSTRACT	18. NUMBER OF PAGES	19a. NAME OF RESPONSIBLE PERSON
a. REPORT **unclassified**	b. ABSTRACT **unclassified**	c. THIS PAGE **unclassified**		**9**	

arrival fluctuations in a lasercom link.[3] These experiments help to understand the atmospheric characteristics over the test range, how they influence a lasercom link, and the ability of atmospheric mitigation techniques to compensate for turbulence induced fluctuations. Experiments have also been performed investigating the spatial profile of the lasercom beam after roundtrip propagation over the test range. These experiments help to understand the degradation of spatial coherence in the laser beam and suggest possible methods for mitigating turbulence effects over the lasercom link.

This manuscript describes the raw data collection and analysis of experiments for measuring spatial degradation of the laser beam transmitted over the NRL Chesapeake Bay lasercom range. Section 2 describes the experimental setup Section 3 presents some raw image files showing instantaneous images of beam profiles after propagation over the 32 km test range. Section 4 describes methods and results of analysis of contiguous image samples to determine spatial correlations across the receiver telescope pupil plane and estimates of aperture averaging over various receiver sizes. Section 5 gives conclusions.

2. EXPERIMENTAL SETUP AND RAW IMAGE DATA

An overview of the test range is shown in figure 1. The transmitter and receiver are located on a 30 m cliff on the western shore of the Chesapeake Bay at NRL-CBD. The transmitted laser beam ($\lambda \approx 1550$ nm) is propagated 16.2 km along a slightly downward path (elevation ~ -1 mrad) to 5 cm diameter corner cube retro-reflectors mounted 15 meters above the water on a tower on Tilghman Island on the eastern shore. The beam is retro-reflected back to the receiver located at CBD where images of the pupil plane are acquired. During all the experiments described in this manuscript, the path averaged atmospheric structure constant, C_n^2, was approximately 2×10^{-15} $m^{-2/3}$, with a corresponding Fried parameter, r_0, of approximately 4 cm.[4] The number and configuration of the retro-reflector array was varied in the experiments to investigate the impact of the various retro-reflector arrangements on the received laser's transverse spatial coherence.

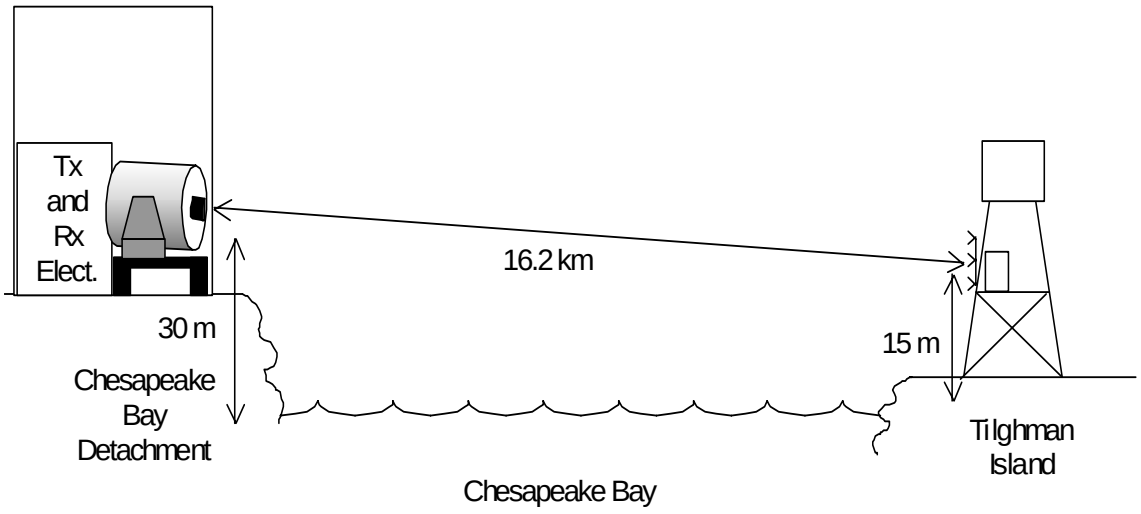

Figure 1: Chesapeake Bay Lasercom Testbed Geometry

The transmitter and receiver arrangement are shown in figure 2. The transmitter consisted of an oscillator, amplifier and collimator to produce the beam for transmission across the bay. The oscillator was a COTS laser diode that produces an output power of 30 mW at a wavelength of 1556 nm in a single mode optical fiber (SMF). The SMF output of the oscillator was coupled to an erbium doped fiber amplifier (EDFA) that amplified the power to 1.6 watts. The SMF output from the EDFA was mounted in a fiber chuck and power out of the fiber was propagated in air from the end of the fiber to a collimating lens. The collimating lens was a 10 cm diameter doublet with a focal length of 24 cm. The output beam transverse profile was measured to be a TEM_{00} Gaussian with no higher order modes discernable, as measured by scanning a 3 mm aperture power meter across the beam. The distance from the output end of the fiber to the 10 cm collimating lens was adjusted with a micrometer to achieve a divergence of ~250 μrad. The fiber chuck and collimating lens assembly were fixed relative to each other and mounted on a remotely controllable Sagebrush gimbal with 35 μrad angular resolution. The transmitter gimbal was mounted below the receiver and aimed through the

mounting forks of the receiver telescope gimbal mount. The transmitted beam axis was approximately 0.4 meters from the central axis of the receiver telescope.

The main optical component of the receiver was a model LX200 Meade telescope. This telescope was a Schmidt-Cassegrain telescope with a 16" primary and a 5" secondary resulting in a total annular collection area of 1170 cm^2. The effective focal length of this telescope was 4 meters at the output flange of the telescope. The telescope included a motorized gimbal for course pointing adjustment. A 10 cm focal length lens at the output of the telescope was used to image the telescope's pupil plane on an InGaAs CCD camera and measure transverse beam profiles of the received beam across the 40 cm aperture of the telescope. The camera was a model SU320MX InGaAs CCD from Sensors Unlimited that consisted of a 320x240 array with 40x40 μm^2 pixels. The 10 cm pupil plane imaging lens and telescope optics resulted in a demagnification of 27.5 on the CCD. Therefore, a single 40x40 μm^2 pixel on the camera mapped to a 1.1x1.1 mm^2 region on the pupil plane. The CCD was capable of running in progressive scan mode at a 60 Hz frame rate with adjustable exposure times per frame of 125 μsec to 16 ms. Transverse positioning of the camera, relative to the axis of the telescope, was iterated with pointing of the telescope to center the camera on the telescope's axis and eliminate obscuration of the beam in the telescope housing. A 1500 nm long pass filter and various ND filters (up to an optical density of 6) were placed in front of the camera to minimize background and achieve best contrast on the CCD.

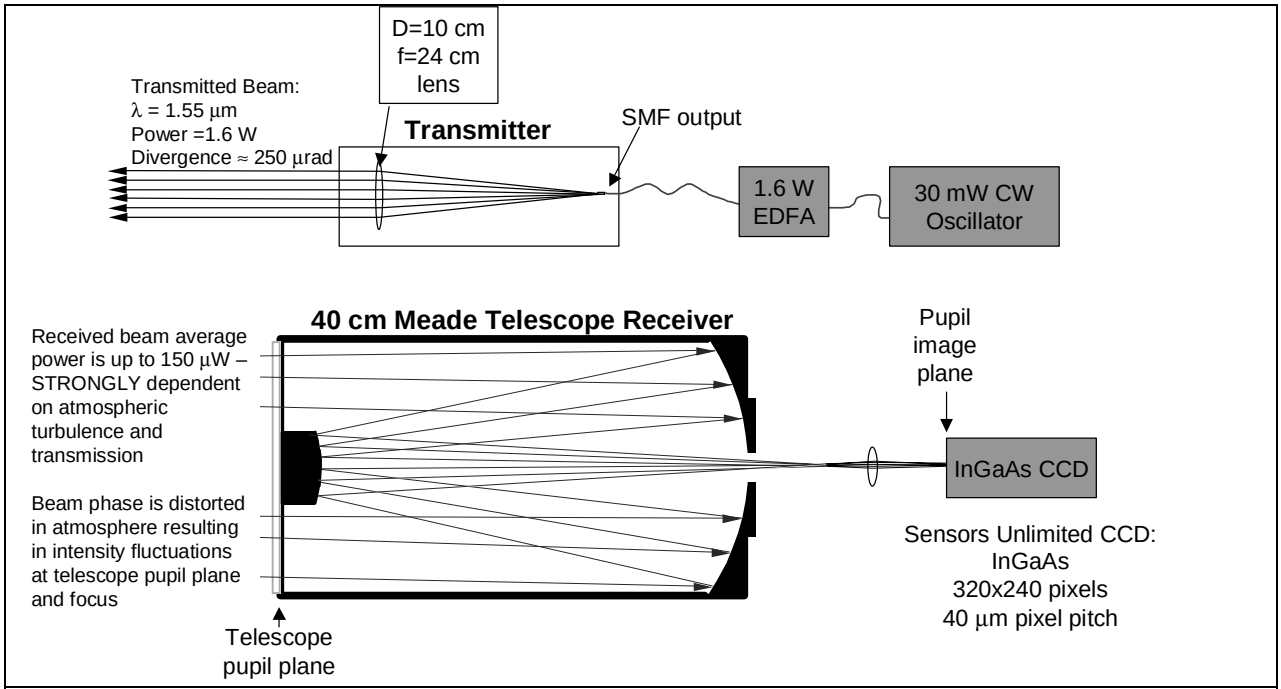

Figure 2: Layout of the bi-static transmitter and receiver arrangement at NRL-CBD. The transmitter was centered approximately 40 cm below the central axis of the receiver telescope

3. RECEIVED BEAM PROFILES

The first test conducted to study spatial profiles of the received beam was investigating the uniformity of illumination of the receiver telescope's pupil plane. Figure 3a shows the average intensity distribution over the telescope pupil plane after reflection from the 5 cm retro-reflectors. This intensity distribution was generated by averaging approximately 3000 images (50 seconds) of the pupil for various configurations of the 5 cm retro-reflectors. As is apparent, there is substantial variation across the pupil plane with the highest intensity received at the edge of the pupil closest to the transmitter. This non-uniform illumination is due to each individual retro-reflector reflecting the laser back to CBD along the axis of the transmitter and not the axis of the receiver. This results in an intensity distribution peaked along the transmitter axis and the outer portion of this distribution being intercepted by the receiver (as shown in figure 3). The retro-reflectors were illuminated by the 250 μrad divergence transmitted beam from CBD, which corresponds to a beam size at the Tilghman Island tower of approximately 4 meters. This large beam size compared to the relatively small size of the retro-reflectors, resulted in nearly uniform illumination of each retro-reflector for long time averages. The beams retro-reflected from these retro-reflectors therefore had a diffraction limited

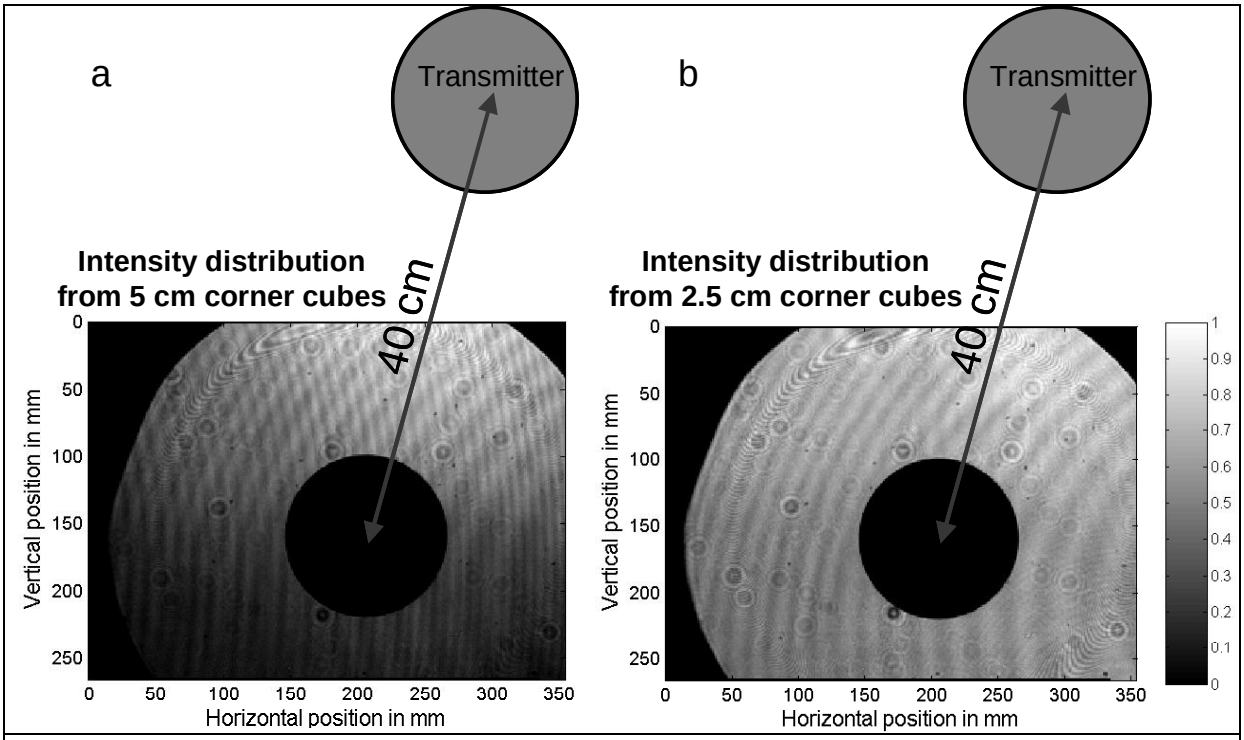

Figure 3: Intensity distributions over the receiver telescope pupil plane averaged over approximately 3000 images or 50 seconds. (a) Distribution returned from 5 cm retro-reflectors. (b) Distribution returned from 2.5 cm retro-reflectors. The drawing of the transmitter aperture shows its location relative to the receiver. In this image and the pupil plane images that follow, there are various artifacts induced by flaws in the collection optics. The arc of fringes observed in the upper left corner of both images are caused by aberrations in the corrector plate of the receiver telescope. The fringes extending throughout the pupil are caused by reflections from the lens used for imaging the pupil plane. The small scale diffraction spots (size ~ 1 cm) are artifacts caused by contaminants on the optics.

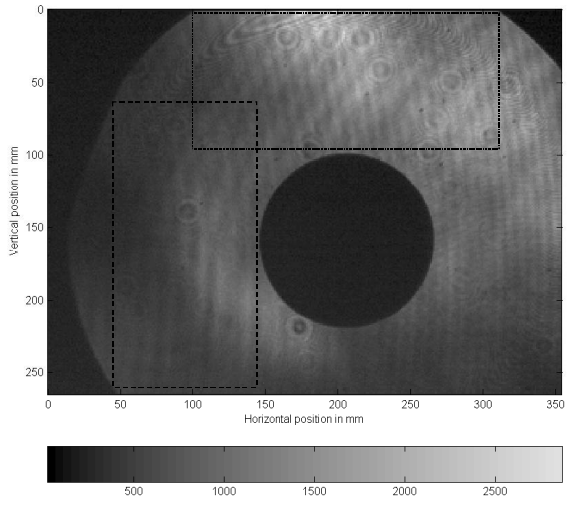

Figure 4: Single frame from InGaAs CCD array showing structure induced in beam profile after reflection from single 5 cm diameter retro-reflector. The horizontal dotted box is the location over which the 2-dimensional correlations, horizontal correlations and aperture averaging factors were calculated in section 4. The vertical dashed box is the location over which the vertical correlations were calculated in section 4.

half-angle divergence of 38 μrad and, neglecting atmospheric effects, Airy disc patterns at NRL-CBD that were all centered on the transmitter with a radius to the first null of approximately 60 cm. This is in agreement with the observed profile that shows a null near the edge of the telescope pupil opposite the transmitter – approximately 60 cm from the transmitter axis. Figure 3b shows a similar experiment performed with 2.5 cm retro-reflectors. In this case, the pupil illumination is much more uniform due to the much larger diffraction angle from these smaller retro-reflectors – half-angle divergence is approximately 76 μrad. This larger divergence results in the first Airy disc null occurring at a 120 cm radius which is well beyond the opposite edge of the telescope at r=60 cm. Therefore, in figure 3b, the portion of the returned beam intercepted by the receiver is well within the central lobe of the Airy disc and much more uniform than the 5 cm retro-reflector case. However, it should be noted, that although the pupil illumination from the 2.5 cm retro-reflectors was much more uniform than from the 5 cm retro-reflectors, the average received power from the 5 cm retro-reflectors was always much greater than from the 2.5 cm retro-reflectors (keeping the number of retro-reflectors fixed). For this reason, all lasercom experiments and the rest of the beam profile studies discussed in this manuscript utilized the 5 cm retro-reflectors.

Another experiment performed was investigation of the instantaneous received beam profiles for various numbers and arrangements of retro-reflectors on the Tilghman Island tower. Figure 4 shows a typical sample of the beam profile after reflection from a single 5 cm retro-reflector. The beam profile shows some bright regions with scale sizes of approximately 5 cm. The image also shows two boxes oriented horizontally and vertically which indicated the locations where all statistical analysis of the beam profiles where performed. These analyses involved calculation of spatial correlations in the received beam profile and estimates of aperture averaging. The results of these analyses are described in section 4.

Figure 5a shows the beam profile observed after reflection from two 5 cm retro-reflectors separated horizontally by 15 inches on the Tilghman Island tower. Interference fringes are clearly visible. These interference fringes are analogous to Young's two slit experiment over a 16.2 km path length. The image shown in figure 5a was selected from a sequence of 300 images to illustrate the existence of fringes. This image displayed the highest contrast of all images in the sequence. Typically, the fringes fluctuated strongly in angle, spacing, shape and contrast due to phase front distortions in the atmosphere, although the fringes were still visible in all but a few frames. Figure 5b shows a horizontal lineout across the boxed region in figure 5a. The lineout is calculated by averaging over all rows within the box. Also shown in figure 5b is the expected spacing of the fringes based on the optical path difference between the two retro-reflectors over the image (assuming propagation in uniform medium). This spacing is expected to be 65 mm, which is slightly larger than observed. This difference is likely due to a systematic error in the calibration of the image scale since the fringe spacing always tended to be on average approximately 10% lower than predicted. Work is ongoing to reconcile this discrepancy.

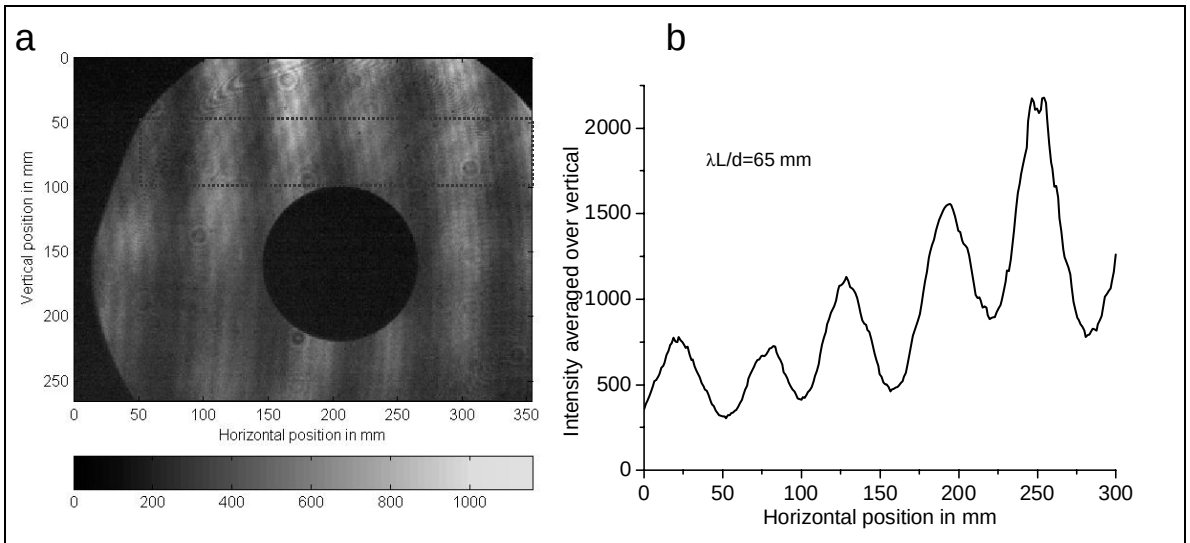

Figure 5: Left: Single frame from InGaAs CCD array showing vertical interference fringes observed after reflection from two 5 cm retro-reflectors separated horizontally by 15 inches on the Tilghman Island tower. Right: Horizontal intensity distribution within dashed box (averaged over rows within box).

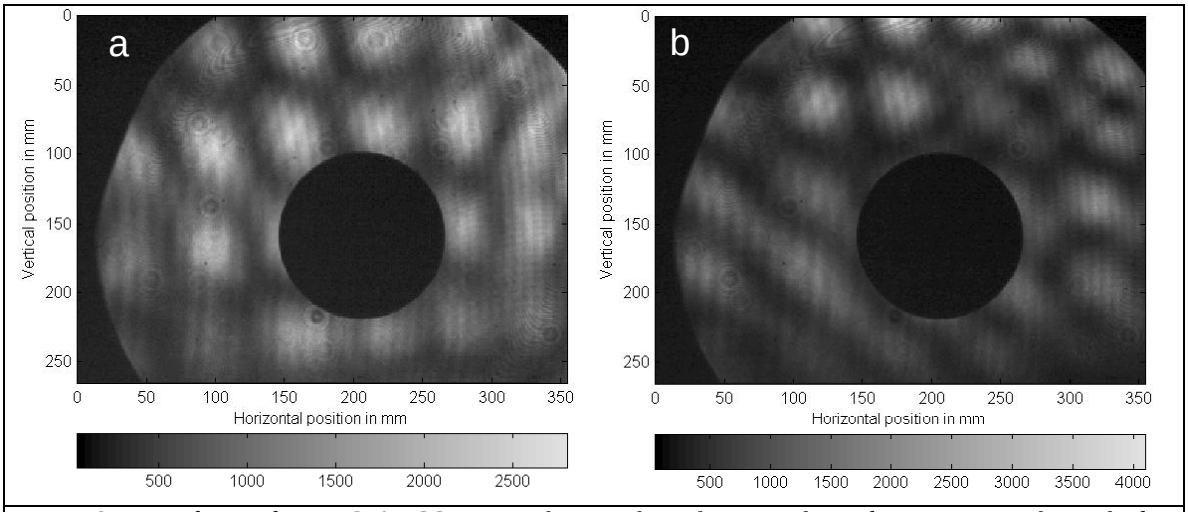

Figure 6: Two frames from InGaAs CCD array showing the 2-dimensional interference pattern observed after reflection from four 5 cm retro-reflectors arranged in a 15 inch square on the Tilghman Island tower.

Figure 6 shows two received beam profiles observed after reflection from four 5 cm retro-reflectors arranged in a square pattern with 15" per side. Both images display a two dimensional interference pattern characteristic of four equally spaced coherent sources. However, the image on the right shows that the interference patterns fluctuate greatly even within a single frame. In the lower left corner of figure 6b, diagonal linear fringes are observed which suggest only the lower left and upper right retro-reflectors were illuminating this portion of the pupil resulting in this two slit interference pattern. In the upper right corner of figure 6b, a 2-dimensional interference pattern similar to figure 6a is observed, but with different spacing and a lower contrast in places. This variation across the pupil shows the complicated paths over which the retro-reflected light travels and the distortion in optical path length induced by the atmosphere.

4. ANALYSIS

The InGaAs CCD acquires multiple snapshots of the beam profile at a 60 Hz rate allowing statistical analysis of an image sequence to determine spatial correlations and estimates of aperture averaging across the pupil plane. Spatial correlations have been calculated by performing auto-correlations of single frame pupil plane images and averaging a long sequence of these correlations to obtain the average transverse spatial correlation of the received beam. The correlations where performed over the boxes shown in figure 4. There were multiple steps performed in the analysis to remove background noise and biases in the images. The first step of analysis involved cropping the pupil images to either the horizontal or vertical box shown in figure 4. In the second step, the entire sequence of images was averaged to obtain an average intensity distribution (similar to averaged profile shown in figure 3) which was then divided into each image. This step was performed for two purposes. The first was to reduce the artifacts in the images from the corrector plate, lens reflections, and optics contaminants as described above. The second reason for dividing by the average intensity distribution was to reduce any bias induced in the correlations due to the non-uniform illumination of the pupil. Without this step, the non-uniform illumination will cause artificial anti-correlations between regions of the image that are bright on average with those that are dark on average. Since we are only interested in statistical fluctuations in the image sequence, this step will not introduce any errors in calculating the correlations. The final step was the calculation of the 2-dimensional correlations. In this step, four 2-dimensional correlations where performed and averaged to give the final correlation. The four correlations were performed using each quadrant of the image (upper-left quarter of image, upper-right quarter of image, lower-right quarter of image, and lower-left quarter of image) as a reference image and correlating these reference images with the image in the entire boxed region.

The results of the correlation calculations are shown in figure 7. The three contour plots shown on the left (Figure 7a, 7b, and 7c) are the 2-dimensional correlations over the horizontal region of the pupil shown in figure 4 for three different configurations of 5 cm diameter retro-reflectors. Figure 7a shows the 2-dimensional correlation for a single retro reflector. Figure 7b shows the 2-dimensional correlation for four retro-reflectors arranged in a 15" square. Figure 7c shows the 2-dimensional correlation for an array of twelve retro-reflectors in a rectangular array with 5" spacing and

an arrangement of 4 rows and 3 columns. This arrangement of twelve retro-reflectors was the arrangement used for lasercom experiments.[2] The two graphs on the right (Figure 7d and 7e) show the 1-dimensional correlations in the horizontal and vertical directions calculated over the respective horizontal and vertical boxed regions shown in figure 4.

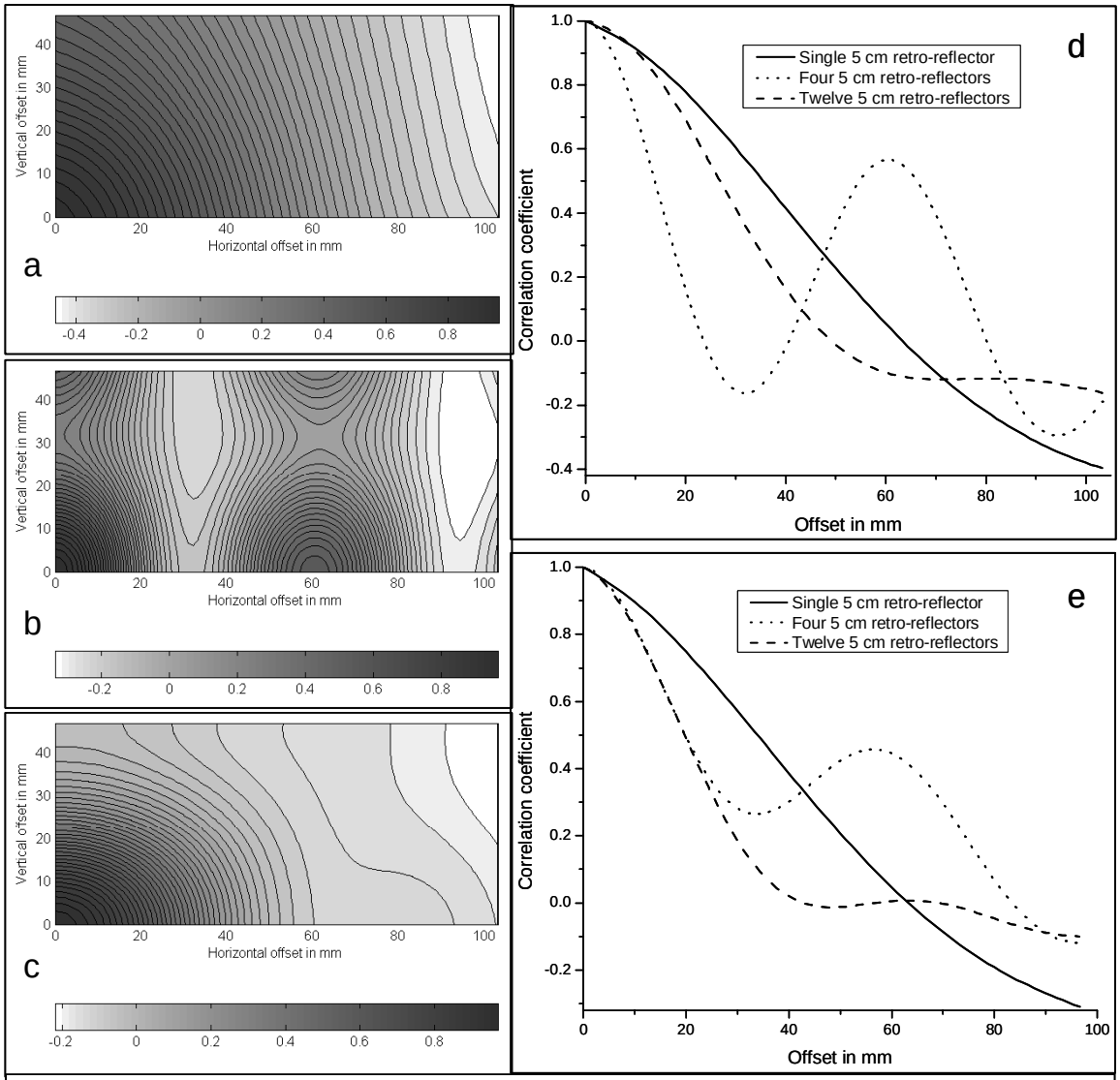

Figure 7: Spatial correlations of the received beam profile. The contour plots are 2-dimensional correlations over the horizontal boxed region shown in figure 4. The line plots are 1-dimensional correlations in the horizontal (7d) and vertical directions (7e). (7a) 2-d correlation of beam received from single 5 cm retro-reflector (7b) 2-d correlation of beam received from four 5 cm retro-reflectors arranged in a 15" square (7c) 2-d correlation of beam received from a 4 row by 3 column array of twelve 5 cm retro-reflectors spaced by 5 inches (7d) Horizontal correlations for the three retro-arrangements in figures 7a-7c. (7e) Vertical correlations for the three retro-arrangements in figures 7a-7c.

These 1-dimensional correlations were calculated by sliding the reference images exclusively in the horizontal or vertical dimension.

The correlations all show significant decrease (~50%) in the correlation coefficient in distances on the order of the Fried parameter (4 cm). However, there is significant structure in the correlations for the cases of four and twelve retro-reflectors. In the case of the square of four retro-reflectors, a strong modulation is observed which is due to the regularly spaced grid of bright and dark spots caused by interference (see figure 6). This regularly spaced intensity

pattern causes enhanced correlation when bright (dark) spots overlap with other bright (dark) spots, and decreased correlation when bright (dark) spots overlap with dark (bright). Similar effects are observed with two retro-reflectors separated horizontally or vertically except, in this case, only the horizontal or vertical correlation component exhibits the modulation. The structure observed in the twelve retro-reflector case is likely due to a similar interference effect except, in this case, the interference pattern is much more complicated due to the large number of retro-reflectors. It is interesting to note that although the three cases shown here have significantly different structure, they all appear to follow the same general trend. That is, the four and twelve retro-reflector cases oscillate around the single retro-reflector case but both fall off, on average, at the same rate as the single retro-reflector case.

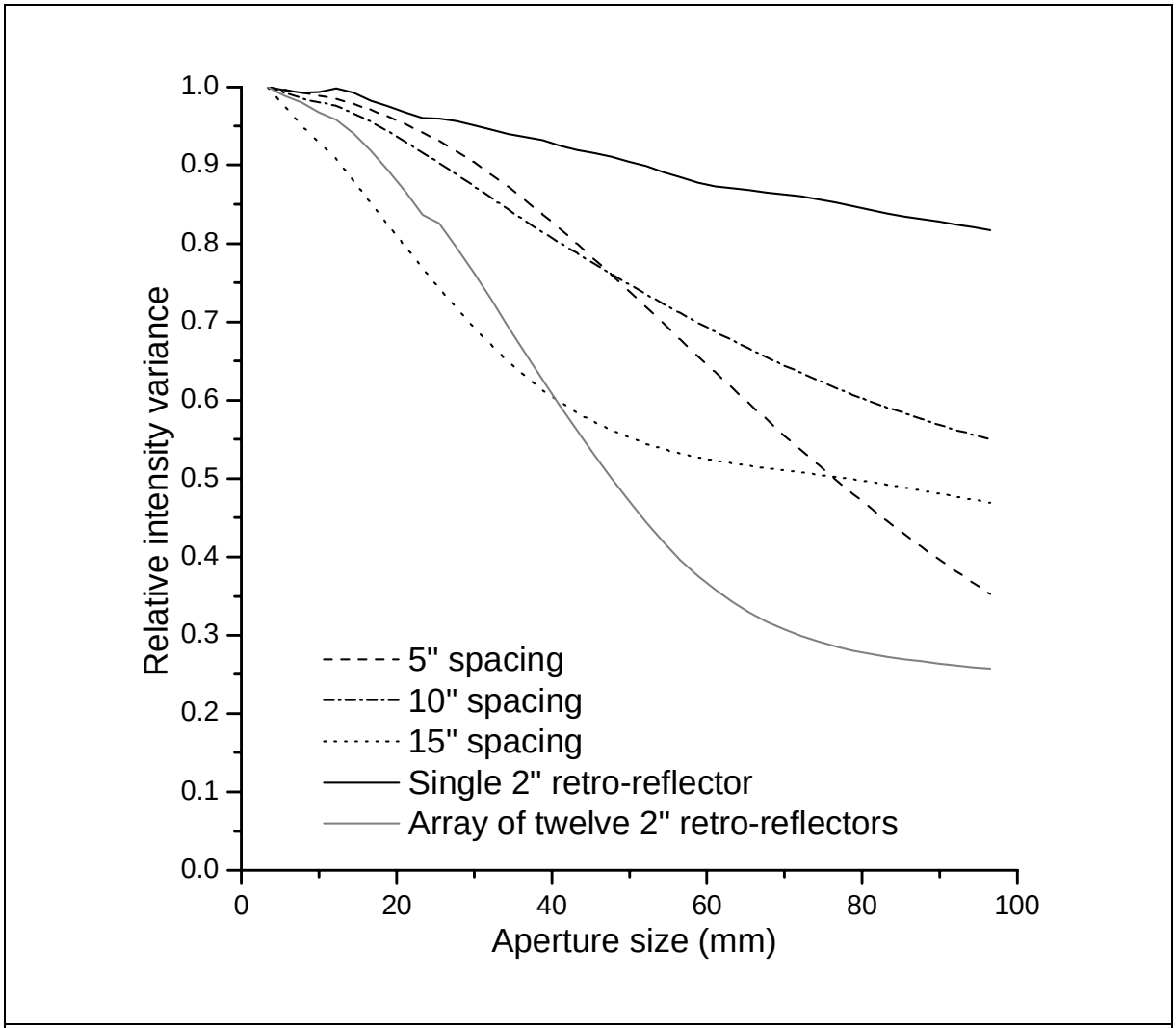

Figure 8: Aperture averaging factor for various retro-reflector configurations. The solid lines are for a single 5 cm retro-reflector (black line) and the array of twelve retro-reflectors used for lasercom experiments (gray line). The dashed/dotted lines are for four 5 cm retro-reflectors arranged in various size squares.

The 3-dimensional nature of the contiguous image samples taken with the CCD, two dimensions in space and one in time, allow analysis of the images to determine the aperture averaging factor[4-7] as a function of aperture size. For this analysis, no pre-processing was done on the images to correct for background or reduce artifacts. The first step in the aperture averaging analysis was to crop the raw images in the contiguous image samples to the horizontal boxed region-of-interest (ROI) shown in figure 4. The second step was the calculation of the variance in time of various size sub-images. For this, a loop starting from a 3x3 pixel matrix and extending to the maximum allowable square matrix within the ROI was performed. For each iteration of the loop, the pixel values within the NxN matrix of each image were

summed and the variance of these single values from each image was calculated over the image sequence in time. This is somewhat, although not completely analogous, to an NxN sized aperture focusing the received light on a single pixel detector (as typically used for lasercom) and calculating the variance of this received signal in time. The reason the analysis described here is not completely analogous to the single pixel receiver case is the lack of phase information contained in the CCD signal which will affect the focusing of the received beam. However, phase information will only effect the distribution of energy in the focal plane and not the total energy received, since energy must be conserved. Therefore, assuming the single pixel detector is large enough to collect all photons falling on the NxN matrix after focusing, the analysis described here accurately describes the single pixel case. The variance calculations of the 3x3 to NxN matrices results in a one-dimensional array with variance as a function of aperture size. Since the correlation calculations above show that a 3x3 pixel matrix (3.3x3.3 mm^2 area in the pupil plane) is much smaller than the transverse spatial correlation length (~ centimeters) in the received beam, the variance of the 3x3 pixel matrix closely approximates the single point variance in the received beam. We can therefore divide all the calculated variances by the 3x3 matrix variance to obtain the aperture averaging factor as a function of aperture size.

Figure 8 shows the results of the aperture averaging factor calculations for various configurations of 5 cm retro-reflectors. The solid black line is the calculated aperture averaging factor for a single 5 cm retro-reflector on the Tilghman Island tower. In this case, very little aperture averaging is observed even for up to a 10 cm square aperture. The solid gray line is the calculated aperture averaging factor for the array of twelve retro-reflectors used for lasercom experiments. In this case, significantly greater aperture averaging is observed than in the single retro-reflector case – twelve retro-reflector array aperture averaging factor is three times greater than the single retro-reflector aperture averaging factor at an aperture size of 60 mm. The dashed lines are the aperture averaging factor for square distributions of 5 cm retro-reflectors with various spacing. No definitive trend is visible for the various size squares of four retro-reflectors, although the four retro-reflector cases tend to lie on average between the single retro-reflector and twelve retro-reflector cases. This suggests that the arrangement of the retro-reflectors is less important than the number of retro-reflectors in improving the aperture averaging factor.

5. CONCLUSIONS

Measurements of the spatial profiles of a retro-reflected laser beam over a 32.4 km lasercom test range have been performed. The spatial profiles were measured over the 40 cm pupil plane of a Meade telescope using an InGaAs CCD array. These measurements were performed for various numbers of retro-reflectors and configurations of retro-reflectors. Received beam profiles after reflection from multiple retro-reflectors show strong interference fringes at retro-reflector separations up to 15 inches (the maximum separation used in experiments). The interference fringes were observed to fluctuate in angle, spacing, and shape due to non-uniform atmosphere over the separate paths traveled from each retro-reflector. Spatial correlation measurements show received beam correlation lengths on the order of predicted atmospheric coherence lengths (~4 cm). Interference fringes from multiple retro-reflectors were observed to cause modulation in the received beams spatial correlation. The spatial correlation modulation induced by interference appears to be super-imposed on a monotonically decreasing correlation that is similar for different numbers of retro-reflectors. The aperture averaging factor for various size apertures has been deduced from the contiguous samples of images obtained with the CCD array. The aperture averaging factor as a function of receive aperture size appears to be strongly affected by the number of retro-reflectors, but not the arrangement of the retro-reflectors.

REFERENCES

1. M.F. Stell, C.I. Moore, H.R. Burris, M.R. Suite, M.J. Vilcheck, M.A. Davis, R. Mahon, E Oh, W.S. Rabinovich, G.C. Gilbreath, W.J. Scharpf, and A.E. Reed, "Passive optical monitor for atmospheric turbulence and windspeed," *Proceedings of the SPIE*, **This issue**, 2003.
2. M.J. Vilcheck, H.R. Burris, C.I. Moore, M.F. Stell, M.R. Suite, M.A. Davis, R. Mahon, E. Oh, W.J. Scharpf, W.S. Rabinovich, A.E. Reed, and G.C. Gilbreath, "Progress in high-speed communication at the NRL Chesapeake Bay Lasercom Facility," *Proceedings of the SPIE*, **This issue**, 2003.
3. M.R. Suite, H.R. Burris, C.I. Moore, M.J. Vilcheck, R. Mahon, M.F. Stell, M.A. Davis, W.S. Rabinovich, W.J. Scharpf, A.E. Reed, and G.C. Gilbreath, "Fast steering mirror implementation for reduction of focal-spot wander in a long-distance free-space communication link," *Proceedings of the SPIE,* **This issue**, 2003.
4. Andrews, Larry C. and Phillips, Ronald L., *Laser Beam Propagation Through Random Media.* SPIE Optical Engineering Press, 1998.
5. Andrews, Larry C., Phillips, Ronald L. and Hopen, Cynthia Y., *Laser Beam Scintillation with Applications.* SPIE Optical Engineering Press, 2001.
6. D.L. Fried, "Aperture averaging of scintillation," *J. Opt. Soc. Am.* **57**, 169-175 (1967).
7. J.H. Churnside, "Aperture averaging of optical scintillations in the turbulent atmosphere," *Appl. Opt.* **30**, 1982-1994 (1991).